

Topology Optimization of a Coupled Aerothermoelastic System



Pankil N. Mishra and Abhijit Gogulapati

1 Introduction

Topology optimization (TO) of structures in multi-disciplinary environments has been explored in a number of studies [1–3]. The present work is motivated by interest in aerothermoelastic applications in which the coupled fluid-thermal-structural interactions (FTSI) play a prominent role. Several previous studies [4–9] have highlighted the importance of the feedback between the aerothermal loads and the structural response.

In particular, this coupling introduces a path dependency into the response problem that creates a wide variety of challenges for both the modeler and the designer. As separate topics of research, topology optimization strategies and aerothermoelastic modeling and analyses have produced a number of publications. However, topology optimization of a coupled aerothermoelastic system has received limited attention.

Reference [10] describes an optimization framework based on a transient adjoint sensitivity analysis approach to obtain optimal configurations of a fully coupled aerothermoelastic system. Finite element-based structural, compressible flow, and transient thermal solvers, are coupled using a monolithic approach. The author however notes that additional work is required before meaningful results can be obtained. Optimization of metallic panels for the flutter and buckling metric was considered in [11]. The structural response was coupled to piston theory-based aerodynamic pressure. However, the temperature of the panel was assumed to be constant throughout the analysis. It was observed that flutter and thermal buckling

P. N. Mishra (✉) · A. Gogulapati

Department of Aerospace Engineering, Indian Institute of Technology Bombay, Powai, Mumbai, Maharashtra 400076, India

e-mail: pankilmishra@iitb.ac.in

A. Gogulapati

e-mail: abhijit@aero.iitb.ac.in

metrics were competing objectives when the panel was subjected to prescribed temperature conditions.

A boundary variation method based on a level-set approach was used to optimize the topology of a static aeroelastic system in [12]. Mass minimization study was carried out with a flutter constraint. The authors note that the optimal designs may be dependent on the initial design itself. An evolutionary-based topology optimization study with stress minimization as the objective is described in [13]. The aerodynamic pressure is described using piston theory. The effect of material degradation on structural response was included. The authors concluded that the optimal configurations were dependent on the effect of material degradation and the application of non-uniform temperature loading resulted in optimal designs governed by thermal stresses. An aerothermoelastic framework was developed by coupling a flexible supersonic wedge to a fluid solver in [14]. The structural optimization of a panel on the wedge for steady state aerothermoelastic response was implemented using gradient-based approach.

It is evident from the review of literature presented above that such a study has not been considered prior to this work. The principal objective of the proposed study is to explore topology optimization of a coupled aerothermoelastic systems. The specific objectives are:

1. To maximize the non-linear normalized thermal buckling metric of the panel using density-based topology optimization approach.
2. To explore the impact of periodic cellular structure using variable linking method on optimal topology with potential applications to manufacturing constraint.

2 Configuration and Modeling

A panel of length L and thickness h shown in Fig. 1 is selected as the structural system. The third dimension of the panel is assumed to be infinitely long and the L/h ratio is fixed as 25. The panel is fixed on both the ends while its top surface is subjected to a hypersonic flow conditions mentioned in Table 1. The panel material is Ti-6Al-2Sn-4Zr-2Mo and thickness is 5 mm.

A basic implicit scheme is used to couple the aerothermoelastic framework developed obtained by coupling finite element-based structural and thermal solvers. The pressure and heat loads are computed using piston theory and Eckert's reference

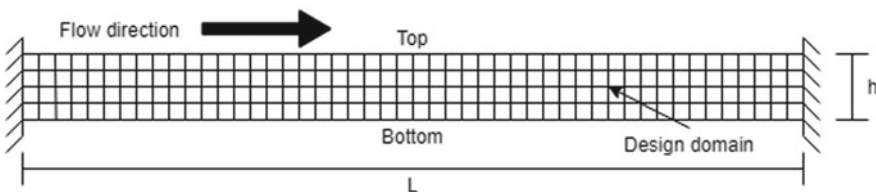


Fig. 1 Schematic of the panel configuration

Table 1 Flow conditions

Property	Value
Free-stream Mach No. (M_∞)	7.0
Altitude	30.0 km
Free-stream pressure (P_∞)	1090 Pa
Free-stream temperature (T_∞)	227 K
Upstream transition to turbulence	1.0 m

enthalpy approaches, respectively [2]. The description of various models is provided in the following subsections.

2.1 Aerodynamic Pressure Model

The aerodynamic pressure p_a at a point along the top surface of the panel is calculated using the third order piston theory given by:

$$p_a = 2 \cdot \frac{q_\infty}{M_\infty} \cdot \left[\left(\frac{1}{U_\infty} \cdot \frac{\partial w}{\partial t} + \frac{\partial w}{\partial x} \right) + M_\infty \cdot \frac{\gamma + 1}{4} \cdot \left(\frac{1}{U_\infty} \cdot \frac{\partial w}{\partial t} + \frac{\partial w}{\partial x} \right)^2 + M_\infty^2 \cdot \frac{\gamma + 1}{12} \cdot \left(\frac{1}{U_\infty} \cdot \frac{\partial w}{\partial t} + \frac{\partial w}{\partial x} \right)^3 \right] \quad (1)$$

where q_∞ is the dynamic pressure, w is the panel displacement in transverse direction, x is the free-stream direction along the flow as shown in Fig. 1 and t is time. Note that the undeformed configuration of the panel is parallel to the free-stream flow.

2.2 Aerodynamic Heating Model

The thermal loads generated due to the flow over the panel's top surface are estimated using the Eckert's reference enthalpy method [15]. The aerodynamic thermal load is determined from the Eq. 2, where U_e , St^* , ρ^* , H_w and H_{aw} are the velocity of the flow at the edge-of-boundary-layer, the Stanton number, density of the flow at the reference condition, the enthalpy at the wall and at the adiabatic wall condition, respectively.

$$Q_{\text{aero}} = St^* \cdot \rho^* \cdot U_e \cdot (H_{aw} - H_w) \quad (2)$$

Note that the coupling between panel deformation and thermal load is incorporated by updating the edge-of-boundary-layer pressure using piston theory, mentioned in Sect. 2.1.

2.3 Finite Element Models

In-house finite element code is used in the present case study. Bi-linear Q4 finite elements are used for both the structural (2 displacement degrees of freedom per node) and thermal (1 temperature degree of freedom per node) solvers discussed below. Identical finite element mesh with consistent matrices are used for both the solvers. More information about the finite element procedure and analysis is available in [16].

2.3.1 Thermal Solver

The finite element formulation of the heat transfer governing equation is used to perform transient thermal analysis of the panel using a *Backward difference* scheme. The thermal load vector \mathbf{R}_{T_n} is computed based on thermal boundary conditions specified for the panel based on a staggered scheme.

$$\left(\frac{\mathbf{C}_T}{\delta t_{AT}} + \mathbf{K}_T \right) \cdot \mathbf{T}_{n+1} = \frac{\mathbf{C}_T}{\delta t_{AT}} \cdot \mathbf{T}_n + \mathbf{R}_{T_n} \quad (3)$$

where δt_{AT} is the thermal time-step. The thermal boundary condition along the top surface includes aerodynamic and radiation heat load. Adiabatic boundary conditions are assumed for remaining surfaces of the panel, unless stated otherwise.

2.3.2 Structural Solver

The element temperature T_e is assumed to be spatially uniform within each finite element e , calculated using the average of nodal temperatures extracted from the vector \mathbf{T} at a given time-step. The elastic stress due to thermal expansion within each element is given by:

$$\sigma_{0_e} = \frac{-\alpha \cdot (T_e - T_{ref}) \cdot E_e}{1 - \nu} \cdot \begin{bmatrix} 1 \\ 1 \\ 0 \end{bmatrix} \quad (4)$$

where α , ν and E_e are the coefficient of thermal expansion, the Poisson's ratio and the elastic modulus of the element, respectively. They are assumed to be independent of the temperature. Note that the stresses produced due to the thermally induced displacements in the panel are not considered in the current study. Thus, the geometric stress stiffness matrix \mathbf{K}_σ of the structure is then obtained using:

$$\mathbf{K}_\sigma = \sum_{e=i}^N \mathbf{G}_e^T \cdot \mathbf{S}_e(\sigma) \cdot \mathbf{G}_e \cdot \mathbf{V}_e \quad (5)$$

Table 2 SIMP model

Relation	Property
$E_e = x_e^3 \cdot E_0$	Elastic modulus
$\mathbf{M} = \sum_e (x_e \cdot \mathbf{M}_e)$	Mass matrix
$\mathbf{C}_T = \sum_e (x_e \cdot \mathbf{C}_{Te})$	Heat capacity matrix
$\mathbf{K}_T = \sum_e (x_e^3 \cdot \mathbf{K}_{Te})$	Thermal conductivity matrix
$\mathbf{K} = \sum_e \left(\frac{x_{\min} + (1-x_{\min}) \cdot x_e^3}{1-\nu^2} \cdot \mathbf{K}_e \right)$	Stiffness matrix
$\mathbf{K}_\sigma = \sum_{e=i}^N \mathbf{G}_e^T \cdot \mathbf{S}_e(\sigma) \cdot \mathbf{G}_e \cdot \mathbf{V}_e$	Geometric stress stiffness matrix

where \mathbf{G}_e , \mathbf{V}_e and \mathbf{S}_e are the shape differentiation matrix, volume of the element and matrix reordering of the element stress σ_{0_e} , respectively.

2.3.3 Thermal Buckling Metric

The stability of the panel in terms of thermal buckling is obtained from the Eigenproblem defined below:

$$\{(\mathbf{K} + \mathbf{K}_\sigma) - \lambda_b \cdot \mathbf{I}\} \cdot \phi_b = \mathbf{0} \quad (6)$$

where \mathbf{K} is the linear stiffness matrix and terms in parentheses comprise a net stiffness matrix \mathbf{K}_{net} . The Eigenvector ϕ_b is associated with the b th eigenvalue λ_b of the net stiffness matrix. Thermal buckling means loss of stability of an equilibrium configuration due to thermal loads. In mathematical terms, \mathbf{K}_{net} becomes singular, i.e., the lowest eigenvalue λ^* obtained from Eq. 7 becomes zero.

$$\lambda^* = \min(\lambda_b) \quad (7)$$

2.4 Solid Isotropic Material with Penalization (SIMP) Model

In density-based SIMP method, each finite element is assigned a relative density x_e , a continuous design variable that varies between x_{\min} (void) to 1 (solid). The material property relations used in the current study based on the SIMP model are given in Table 2.

3 Sensitivity Analysis

The design derivatives required for the topology optimization problem are calculated analytically. The adjoint-based sensitivity analysis provides the design derivatives of the thermal buckling metric shown below:

$$\frac{d\lambda^*}{d\mathbf{x}} = \frac{(\boldsymbol{\phi}_b)^T \cdot \left(\frac{\partial \mathbf{K}}{\partial \mathbf{x}} + \frac{\partial \mathbf{K}_\sigma}{\partial \mathbf{x}} \right) \cdot (\boldsymbol{\phi}_b)}{(\boldsymbol{\phi}_b)^T \cdot \mathbf{I} \cdot (\boldsymbol{\phi}_b)} + (\boldsymbol{\beta}_T)^T \cdot \left(\frac{\partial \mathbf{C}_T}{\partial \mathbf{x}} \cdot \left(\frac{\mathbf{T}_x - \mathbf{T}_c}{\delta \mathbf{t}_{AT}} \right) + \frac{\partial \mathbf{K}_T}{\partial \mathbf{x}} \cdot \mathbf{T}_x \right) \quad (8)$$

where the adjoint vector $\boldsymbol{\beta}_T$ is obtained from:

$$\left(\frac{\mathbf{C}_T}{\delta \mathbf{t}_{AT}} + \mathbf{K}_T \right) \cdot \boldsymbol{\beta}_T = - \frac{(\boldsymbol{\phi}_b)^T \cdot \frac{\partial \mathbf{K}_\sigma}{\partial \mathbf{T}_x} \cdot (\boldsymbol{\phi}_b)}{(\boldsymbol{\phi}_b)^T \cdot \mathbf{I} \cdot (\boldsymbol{\phi}_b)} \quad (9)$$

4 Topology Optimization Methodology

The current study is inspired based on the work carried out in [11, 21]. The design variables $\tilde{\mathbf{x}}$ are assigned to finite elements of a unit cell. A variable linking sparse mapping matrix \mathbf{G} defined in Eq. 10, links the design variables of the unit cell to finite elements of other cells in the structural system [17].

$$\mathbf{G} = \begin{bmatrix} 1 & 0 & \dots & 0 & \dots \\ 0 & 1 & \dots & 0 & \dots \\ \vdots & \vdots & \ddots & \vdots & \vdots \\ 1 & 0 & \dots & 0 & \dots \\ 0 & 1 & \dots & 0 & \dots \\ \vdots & \vdots & \ddots & \vdots & \vdots \\ 0 & 0 & \dots & 1 & 0 \\ 0 & 0 & \dots & 0 & 1 \end{bmatrix}_{N_e \times n_e} \quad (10)$$

where N_e is the total number of finite elements in the whole design domain and n_e is the number of finite elements in the single design cell, i.e., the number of design variables $\tilde{\mathbf{x}}$. If the density of element j is linked to the i -th design variable then $\mathbf{G}(j, i) = 1$

A density filter [18, 19] is used to obtain the element densities \mathbf{x} from the design variables $\tilde{\mathbf{x}}$ using the density filter \mathbf{H} . Note that the density filter is applied on to the whole design domain. The topology optimization is performed using the below mentioned steps:

1. Initialization of design variables and set $i = 0$
2. Map the design variables to the whole domain using matrix \mathbf{G}
3. Apply the density filter to obtain the element densities from the design variables

4. Perform the aerothermoelastic analysis for the stipulated simulation time, N_s seconds or till the thermal buckling event happens
5. Perform the sensitivity analysis and map it to the design variables using transpose of the matrix \mathbf{G}
6. Perform optimization of Eq. 11 using MMA algorithm [20]
7. Update the design variables and set $i = i + 1$
8. Perform the steps 2-7 till the convergence criteria is fulfilled.

The objective function is to maximize the normalized thermal buckling metric, where the baseline thermal buckling metric $\lambda_{\text{baseline}}^*$ is calculated once initially for the baseline design domain shown in Fig. 2. The mathematical formulation of the topology optimization problem considered here is shown below:

$$\begin{aligned}
 &\text{Maximize } \frac{\lambda^*}{\lambda_{\text{baseline}}^*} \\
 &\text{w.r.t. } \tilde{\mathbf{x}} \\
 &\text{subject to } \mathbf{v}^T \cdot \mathbf{x} \leq \mathbf{V}^* \\
 &\quad \tilde{x}_e \in [x_{\min}, 1] \quad \mathbf{e} = 1, \dots, N_e
 \end{aligned} \tag{11}$$

where V^* is the volume constraint on the element densities \mathbf{x} . The density filter radius reduces each time the iterations converge within the specified tolerance, according to the following sequence [3.1, 2.9, 2.3, 2.1, 1.5, 1.1, 1.0, 0.1]. The optimization algorithm terminates either when the number of iterations are equal to N_I or when the filter radius value is less than 1.0

5 Results and Discussion

The value of various parameters related to the topology optimization problem are given in Table 3. Note that the flow is over the undeformed (flat) panel which means that effect of pressure load is not considered since the focus is on thermal-structural coupling.

Table 3 Common parameters

Parameter	Value
Number of elements	1600
Max. number of iterations, N_I	700
Min. change	0.0001
Volume fraction, V^*	0.350
Thermal time-step, δt_{AT}	0.1 s
Reference temperature, T_{ref}	300 K



Fig. 2 Topology of baseline design and initial design for case study A

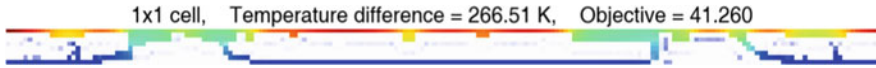


Fig. 3 Optimal topology for case study-A, $N_s = 3 s$

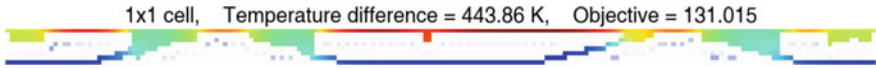


Fig. 4 Optimal topology for case study-A, $N_s = 6 s$

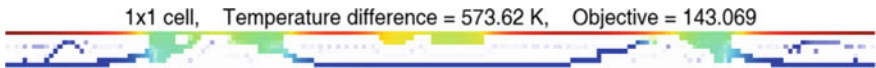
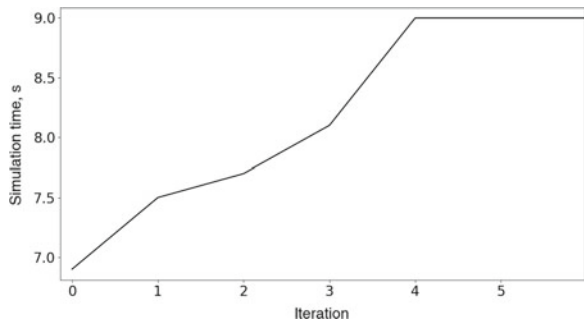


Fig. 5 Optimal topology for case study-A, $N_s = 9 s$

Fig. 6 Simulation time of initial iterates for case study A, $N_s = 9 s$



The topology optimization problem Eq. 11 is solved here for the case study A with an implicit periodic cell constraint as shown in Fig. 2. The optimal topology obtained for the simulation time of 3 s, 6 s and 9 s are shown in Figs. 3, 4 and 5, respectively. The temperature distribution is shown using the *jet* color scheme, where the *red* color indicates the maximum temperature and the *blue* color indicates the minimum temperature across the panel.

The thermal buckling of baseline design takes place at 3.4 s. Due to which the change in objective function value from simulation time of 3–6 s is quite large as compared to that of 6–9 s. As mentioned earlier, the analysis module terminates either when the stipulated simulation time, N_s seconds is achieved or when the thermal buckling of the panel occurs. For simulation time of 9 s, the iterate $i = 0$ terminates at 6.8 s due to the thermal buckling of the panel as shown in Fig. 6. One can observe that the thermal buckling of the panel is delayed and from iterate $i = 4$

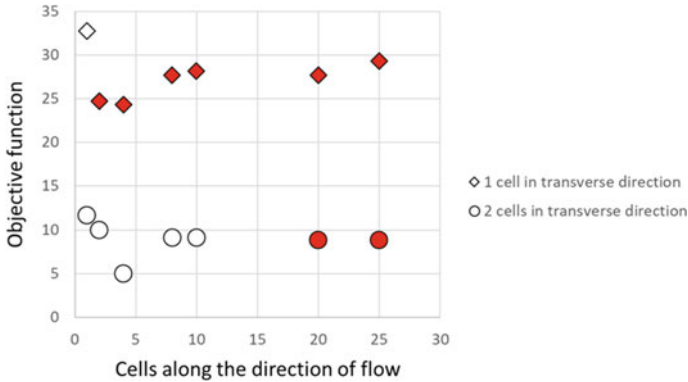


Fig. 7 Objective function for different periodicity

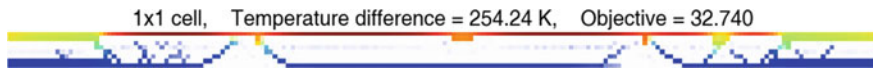


Fig. 8 Optimal topology for 1 × 1 periodic cell

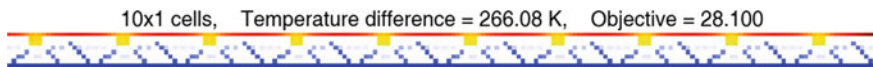


Fig. 9 Optimal topology for 10 × 1 periodic cells

on-wards the analysis module terminates only when the stipulated simulation time of 9 s is achieved.

The design space of case study A ($N_s = 3s$) for different periodic cell structure is shown in Fig. 7. The solid red markers as compared to solid white markers produced configurations where the top and bottom part of the panel were disconnected from each other. The heat transfer from top to bottom takes place through conduction in the internal part of the panel. The absence of internal radiation model leads to the removal of material just below the solid top surface of the panel. They are mathematically feasible solutions to the topology optimization problem Eq. 11 as the thermal buckling metric is calculated for the whole panel (Fig. 8). The panel configuration obtained for 10 × 1 periodicity shown in Fig. 9 is an example of the topology denoted by solid red markers in Fig. 7.

The value of objective function in Fig. 7 is highest for a 1 × 1 periodicity while it decreases as the number of cells in the transverse direction increase from 1 to 2. This is mainly due to the presence of material in middle part which reduces the thermal buckling characteristic of the panel. For example the objective metric of topology 1 × 2 periodicity as shown in Fig. 10 is almost one-third of that for 1 × 1 periodicity as shown in Fig. 8. The optimal topology obtained for 8 × 2 and 10 × 2 periodicity resembles to traditionally manufactured stiffened panels found in aerospace applications shown in Figs. 11 and 12, respectively.

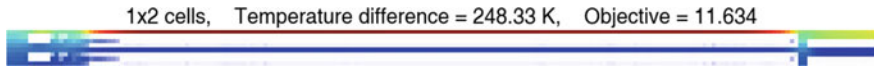


Fig. 10 Optimal topology for 1×2 periodic cells



Fig. 11 Optimal topology for 8×2 periodic cells



Fig. 12 Optimal topology for 10×2 periodic cells

6 Conclusions

Topology optimization for a normalized thermal buckling metric of a 2-D panel heated by the flow is described. The effect of periodic cell constraint on the panel topology is considered implicitly using variable linking method. The investigations revealed the following insights:

- Normalizing of the objective function metric improves the rate of order of convergence 2 to 3 times as compared to non-normalized metric
- Overall the thermal buckling metric of the panel decreases with increase in the periodicity
- Panel configurations with top and bottom part being disconnected are produced due to the absence of internal radiation model
- Periodicity as a manufacturing constraint generates configuration similar to traditionally manufactured stiffened aerospace panels at the cost of optimal panel topology.

Acknowledgements The authors acknowledge the Department of Aerospace Engineering, IIT Bombay for the computational resources and wall time.

References

1. McNamara JJ, Friedmann PP (2011) Aeroelastic and aerothermoelastic analysis in hypersonic flow: past, present, and future. *AIAA J* 49(6):1089–1122
2. Culler AJ, McNamara JJ (2010) Studies on fluid-thermal-structural coupling for aerothermoelasticity in hypersonic flow. *AIAA J* 48(8):1721–1738
3. Gogulapati A, Brouwer KR, Wang X, Murthy R, McNamara JJ, Mignolet MP (2017) Full and reduced order aerothermoelastic modeling of built-up aerospace panels in high-speed flows. In: 58th AIAA/ASCE/AHS/ASC structures, structural dynamics, and materials conference, p 0180
4. Bendsoe MP, Sigmund O (2013) *Topology optimization: theory, methods, and applications*. Springer Science & Business Media

5. Sigmund O, Maute K (2013) Topology optimization approaches. *Struct Multidiscip Optim* 48(6):1031–1055
6. Feppon F, Allaire G, Dapogny C, Jolivet P (2020) Topology optimization of thermal-fluid-structure systems using body-fitted meshes and parallel computing. *J Comput Phys* 417:109574
7. Deaton JD, Grandhi RV (2014) A survey of structural and multidisciplinary continuum topology optimization: post 2000. *Struct Multidiscip Optim* 49(1):1–38
8. Wang X, Xu S, Zhou S, Xu W, Leary M, Choong P, Qian M, Brandt M, Xie YM (2016) Topological design and additive manufacturing of porous metals for bone scaffolds and orthopaedic implants: a review. *Biomaterials* 83:127–141
9. Liu J, Gaynor AT, Chen S, Kang Z, Suresh K, Takezawa A, Li L, Kato J, Tang J, Wang CC et al (2018) Current and future trends in topology optimization for additive manufacturing. *Struct Multidiscip Optim* 57(6):2457–2483
10. Howard MA (2010) Finite element modeling and optimization of high-speed aerothermoelastic systems. Ph. D. Thesis, Colorado University
11. Stanford B, Beran P (2013) Aerothermoelastic topology optimization with flutter and buckling metrics. *Struct Multidiscip Optim* 48(1):149–171
12. Dunning PD, Stanford B, Kim HA (2015) Level-set topology optimization with aeroelastic constraints. In: 56th AIAA/ASCE/AHS/ASC structures, structural dynamics, and materials conference, p 1128
13. Munk DJ, Verstraete D, Vio GA (2017) Effect of fluid-thermal-structural interactions on the topology optimization of a hypersonic transport aircraft wing. *J Fluids Struct* 75:45–76
14. Smith LJ, Halim LJ, Kennedy G, Smith MJ (2021) A high-fidelity coupling framework for aerothermoelastic analysis and adjoint-based gradient evaluation. In: AIAA Scitech 2021 Forum, p 0407
15. Eckert E (1956) Engineering relations for heat transfer and friction in high-velocity laminar and turbulent boundary-layer flow over surfaces with constant pressure and temperature. *Trans ASME* 78(6):1273–1283
16. Cook RD et al (2007) Concepts and applications of finite element analysis. Wiley
17. Kai W, Sigmund O, Jianbin D (2021) Design of metamaterial mechanisms using robust topology optimization and variable linking scheme. *Struct Multidiscip Optim* 63:1975–1988
18. Bruns TE, Tortorelli DA (2001) Topology optimization of non-linear elastic structures and compliant mechanisms. *Comput Methods Appl Mech Eng* 190(26–27):3443–3459
19. Bruns T (2005) A reevaluation of the SIMP method with filtering and an alternative formulation for solid-void topology optimization. *Struct Multidiscip Optim* 30(6):428–436
20. Svanberg K (1987) The method of moving asymptotes | a new method for structural optimization. *Int J Numer Methods Eng* 24(2):359–373
21. Mishra PN, Gogulapati A (2021) Topology optimization of fully coupled aerothermoelastic system. In: Proceedings of the international conference on multidisciplinary design optimization of aerospace systems (AEROBEST 2021), p 192